

Electron Injection, Recombination and Halide Oxidation Dynamics at Dye-sensitized TiO₂ Interfaces

Todd A. Heimer and Edwin J. Heilweil

National Institute of Standards and Technology, 100 Bureau Dr., Stop 8441, Gaithersburg MD 20899

Carlo A. Bignozzi

Department of Chemistry, University of Ferrara, Via L. Borsari 46, 44100 Ferrara Italy

Gerald J. Meyer

Department of Chemistry, Johns Hopkins University, 3400 N Charles St, Baltimore MD 21218

Time-resolved infrared measurements indicate ultrafast, < 350 fs electron injection from (4,4'dcb)₂Ru(NCS)₂ (**1**) and (5,5'dcb)₂Ru(NCS)₂ (**2**) to nanostructured TiO₂ electrodes. {(4,4'dcb) = (4,4'-COOH-2,2'-bipyridine)} Although rapid, the injection from **2** apparently occurs with a lower quantum yield, explaining a lower overall photon-to-current efficiency for **2**/TiO₂ solar cells. Transient visible spectroscopy reveals similar rates of both halide oxidation and injected electron-oxidized dye recombination for the two sensitizers. Substituting SnO₂ for TiO₂ increases the electron injection yield from **2** in the case of transparent metal oxide films and improves the photon to current efficiency. Results indicate competition between electron injection and vibrational relaxation of the sensitizer excited state.

Introduction

Recent transient infrared measurements indicate that interfacial electron injection from the excited state of ruthenium polypyridyl sensitizers to TiO₂ electrodes occurs on the ultrafast (<1 ps) time scale.¹ This suggests electron injection can effectively compete with excited state decay of the sensitizer, however this does not always yield efficient photocurrent production. A second competition exists between recombination of injected electrons with the oxidized Ru^{III} center and halide oxidation by Ru^{III}. This competition has been directly monitored by measuring the rate of Ru^{II} recovery in the presence and absence of I⁻ using transient visible absorbance spectroscopy. Studies of two related sensitizers with significantly different excited state reduction potentials and photovoltaic efficiencies, (4,4'dcb)₂Ru(NCS)₂ (**1**) and (5,5'dcb)₂Ru(NCS)₂ (**2**), suggest limitations and possible methods to improve the performance of dye-sensitized TiO₂ regenerative solar cells.

Photocurrent measurements for (5,5'dcb)₂Ru(X)₂, (where X = NCS⁻, CN⁻ or Cl⁻) on opaque TiO₂ nanostructured electrodes were part of a previous study.² These sensitizers were designed to enhance the spectral sensitivity of molecular solar cells toward longer wavelengths of light. Sensitizers utilizing the 5,5'dcb ligands have significantly lower excited state reduction potentials compared to the corresponding

4,4'dcb analogues, which manifests in red-shifted absorbance spectra. This in turn improves the overlap of the absorbance spectra with the solar spectrum. The sensitizers in this series were compared with the 4,4'dcb analogues and in general displayed maximum incident photon-to-current conversion efficiencies (IPCE) approximately one-half that of the 4,4'dcb sensitizers. Specifically, for **1** and **2** the maximum monochromatic IPCEs were 67.1 % and 36.6 % respectively. It was concluded that the lower IPCE for **2** was due, at least in part, to a lower quantum yield for electron injection from the sensitizer excited state to the TiO₂ as non-radiative decay competes with electron injection.

Scheme 1 displays the relative energetics for **1** and **2** at the sensitizer-semiconductor interface.³ Forward reactions which result in the production of photocurrent are electron injection (with rate constant k_2) and reduction of the oxidized sensitizer by a solution electron donor (k_4). Competing loss mechanisms include excited state decay (k_{-1}) and recombination of injected electrons with the oxidized sensitizer (k_3). The excited state reduction potential of **2** (measured in solution) lies approximately 200 mV positive of that for **1**, resulting in a significant red shift in the absorbance spectrum. The conduction band of single crystal SnO₂ lies approximately 300 mV lower in energy than that of TiO₂,⁴ which may result in enhanced orbital overlap between the excited state of **2** and acceptors in the SnO₂.

Through the recent development of transparent TiO₂ films and the use of time-resolved infrared spectroscopy (TRIR), we are now able to quantify the electron transfer rates at the semiconductor-sensitizer interface for **1** and **2** and make direct conclusions about the competitions between loss mechanisms and forward reactions. These results reinforce the findings of the previous work, and also provide further insight into the fascinating nature of the sensitized metal oxide interface.

Experimental

Materials. Transparent TiO₂ films consisting of ≈16 nm diameter TiO₂ particles were prepared by hydrolysis of Ti(i-OPr)₄ as described previously.⁵ Insulating ZrO₂ films were prepared from Zr(i-OPr)₄ in a similar fashion.⁶ Transparent SnO₂ films were prepared using a slight modification of a published procedure:⁷ One drop of Triton X-100 surfactant was added to 1 mL of 15% SnO₂ colloidal solution (Alfa). This mixture was deposited on the substrate and spread with a glass rod over an area masked with Scotch tape. Two to five applications with 1 hour room temperature drying intervals were required to prepare SnO₂ films approaching 1 μm thick. Final sintering was performed at 400 C for 1 hour in air for all metal oxide films. Indium doped tin oxide conductive glass substrates (Hartford Glass, 8 Ω/sq)⁸ were used for transient visible experiments and photocurrent measurements. Unpolished CaF₂ substrates were used to prepare samples for mid-IR measurements.⁹ Sensitizer **2** was available from previous studies.² Purified **1** was obtained from Greg Smestad, of SolIdeas. Both sensitizers exhibited a single exponential photoluminescence decay in MeOH upon laser excitation at 532 nm, indicating acceptable purity. Attachment of the sensitizers to the TiO₂ surface was achieved by soaking the TiO₂ films in MeOH solutions containing ≈ 5 mM concentration of the sensitizer for 16 hours.

Transient spectroscopy. Time-resolved infrared (TRIR) experiments were performed under the following conditions: The sample was excited at 20Hz with 8 μJ of 590 nm, 150 ps fwhm synch pumped dye laser output. The probe pulse consisted of a broadband ($1850\text{ cm}^{-1} \pm 100\text{ cm}^{-1}$) 250 fs pulse generated by difference frequency mixing of two visible pulses in LiIO_3 . The pump beam and probe beams were focused to approximately 200 μm diameter at the sample. Broadband detection of the probe was achieved directly using a 42 groove/mm single grating spectrograph coupled to a 256 x 256 element InSb array. The pump-probe cross correlation, measured in a Si wafer, indicates an ≈ 350 fs instrument response function. Sample mounting was achieved by using the sensitized TiO_2 samples on CaF_2 as windows in a standard demountable IR cell. The cell was filled with dichloromethane such that the active area of the sample was bathed in the liquid. Further details of the TRIR experiment can be found elsewhere.¹⁰

Transient visible absorbance experiments were performed using a Xe flashpack to produce white light broadband probe pulses of $\approx 3\ \mu\text{s}$ duration. A Q-switched Nd:YAG laser was used to provide 5 ns fwhm excitation pulses at 532 nm. A double monochromator and PMT were used for probe wavelength selection and detection. The system has a temporal instrument response of 14 ns.

To measure decay times on a shorter time scale, an alternate setup was used when required. A Quantel Nd:YAG producing 30 ps fwhm 532 nm pulses was used to excite the sample. This also pumped a dye laser to provide 20 ps fwhm probe pulses. The dye laser was tuned to the wavelength of interest, typically 700 nm, and a CCD was used for detection. The probe was delayed relative to the pump via an optical delay stage.

Photoelectrochemistry. Photocurrent measurements were performed by assembling the sensitized metal oxide electrode against a Pt coated counter electrode, with a thin layer of 0.5 M NaI and 0.05 M I_2 electrolyte in propylene carbonate between the electrodes. A 150 W Xe lamp and single grating monochromator served as the excitation source. Lamp output as a function of wavelength was measured with a NIST calibrated Si photodiode.¹¹

Results

Time-resolved infrared (TRIR) experiments. It has recently been established that transient near IR to mid IR spectroscopy is an effective technique to measure the injection dynamics of electrons in sensitized semiconductors.¹ For sensitized TiO_2 samples following visible excitation, the absorbance by electrons in the TiO_2 is flat across the entire probed region ($1850 \pm 50\text{ cm}^{-1}$) and the average value as a function of time is shown in Figure 1. This region was chosen as it is free from sensitizer excited state absorbance changes, namely the $\nu(\text{C}=\text{O})$ shift^{1b} near 1730 cm^{-1} and the $\nu(\text{C}\equiv\text{N})$ shift near 2100 cm^{-1} . For both **1** and **2** anchored to TiO_2 the 1850 cm^{-1} absorption rise tracks the single-sided cross-correlation with no further increase in intensity, indicating that electron injection is complete within the excitation laser pulse duration. This allows us to place a lower limit for k_2 of 1/350 fs. A TRIR instrument-limited rise-time for **1** on TiO_2 has previously been observed by other research groups, with responses as fast as 25 fs.^{1a}

The coincidence of the cross-correlation and the electron absorbance rise-time caused us to suspect that two-photon excitation of the TiO_2 could give rise to the

observed signal. Substitution of non-sensitized TiO₂ for the sample revealed a small absorbance change ($\Delta\text{Abs} = +0.005$ at 8 μJ pump energy) contribution by this effect, indicated by the arrow in Figure 1. However, the absorbance signal for **1** anchored to TiO₂ exceeds this value by a factor of four, and displays a linear dependence on pump power in the range of 3-12 μJ . The two-photon signal for non-sensitized TiO₂ is undetectable at 3 μJ . No transient absorbance was observed in the 1800-1900 cm^{-1} region for the dye molecules anchored to insulating ZrO₂, indicating that the observed transient absorbance in TiO₂ is not a thermal effect.

Transient visible spectroscopy – (4,4'-dcb)₂Ru(NCS)₂. For the sensitizers anchored to transparent TiO₂ or ZrO₂ films, transient visible spectra are readily obtained. Figure 2 displays the spectra of **1** on ZrO₂ at various times following the excitation pulse. Key features are the MLCT bleach centered at 520 nm, a ligand based absorbance band at 650 nm, and photoluminescence (PL) at 760 nm. These features are all typical of the excited state of **1**.¹² The spectra obtained for **1** on TiO₂ are significantly different, particularly in the near-IR. There is no measurable PL, instead a long lived (tens of μs) positive absorbance persists. This has been attributed to absorbance by electrons injected into TiO₂.^{1a,15} The contribution of the oxidized state of **1** to the near-IR absorbance remains a matter of controversy.^{1a,12}

Recombination of injected electrons with the oxidized dye is measured by monitoring the recovery of the Ru^{II} ground state absorbance at 590 nm. At this wavelength, there is no contribution by the excited state of **1**, as shown by the transient spectra on ZrO₂. Figure 3 displays the observed recovery kinetics as a function of excitation irradiance. As the irradiance is increased beyond 50 μJ , a fast component becomes apparent. Such behavior has been previously observed in this system.¹³ The recovery kinetics are modeled as the sum of a first order and second order decay, and fit to the following equation:

$$I(t) = \alpha_a \exp(-k_a t) + \left[\frac{1}{\alpha_b} + k_b t \right]^{-1}$$

Here k_a and k_b are the first and second order rate constants respectively, and α_a and α_b are the corresponding amplitudes. The observed second order rate constant, k_b , is a function of both the extinction coefficient change ($\Delta\epsilon$) and the optical path length (l) such that $k_b(\text{observed}) = k_b(\text{actual})/(\Delta\epsilon \cdot l)$. We do not have an evaluation of $\Delta\epsilon$, thus only the value for $k_b(\text{observed})$ will be reported here. The rates are summarized in Table 1.

Ru^{II} recovery was also measured in the presence of iodide electron donors in solution. When NaI is added, recovery is much faster, as shown by the kinetic traces in Figure 4a. Addition of both NaI and I₂ as a redox pair allows formation of I₃⁻. This has a dramatic effect on the Ru^{II} recovery in that at 0.25 M NaI and 0.025 M I₂, 90% of the transient signal is quenched within the laser pulse (Figure 4b). This indicates a static quenching mechanism, most likely by adsorbed I₃⁻. The degree of quenching is non-linear in NaI and I₂ concentration, and presumably in [I₃⁻]. In fact the quenching vs. donor concentration fits the Langmuir adsorption isotherm model (Figure 4 inset), with two assumptions: 1) the degree of quenching is proportional to the number of moles of adsorbed I₃⁻, 2) the number of moles of adsorbed species is much smaller than the

number of moles of solution species prior to adsorption, such that $[I_3^-]_{eq} \approx [I_3^-]_0$. These assumptions are necessary, as we are unable to quantitate the concentration of adsorbed species.

Transient visible spectroscopy – (5,5'dcb)₂Ru(NCS)₂ For **2** in solution or anchored to metal oxide films, transient visible spectra are shown in Figure 5. The most prominent feature for the sensitizer in MeOH or on ZrO₂ (Figure 5a) is a positive absorbance at 400 nm, assigned to (5,5'dcb)⁻. This absorbance somewhat overwhelms the MLCT bleach near 540 nm. A second ligand based absorbance appears in the 600-700 nm region. The decay of all features occurs on the timescale of the instrument response (≈ 14 ns). This is expected, since the excited state lifetime of **2** in MeOH is 250 ± 25 ps (data not shown). The spectra for **2** anchored to semiconducting metal oxide films are shown in Figure 5b. For TiO₂ films sensitized with **2**, the spectrum is very similar to ZrO₂ except at times > 20 ns, where a μ s lived positive absorbance persists in the near IR. When **2** is attached to SnO₂ films, the resulting transient spectra are significantly altered. The (5,5'dcb)⁻ absorbance at 400 nm is absent, and the MLCT bleach and near IR absorbance are both enhanced. The lifetime of these features is several μ s.

In the absence of a strong bleach signal for **2** on TiO₂, recombination of injected electrons with the oxidized dye was measured by monitoring the decay of the electron absorbance at 820 nm. Here the contribution from the sensitizer excited state is minimal. At an irradiance of 50 μ J, a second order decay is observed which persists for tens of μ s. The results are shown in Figure 6 and compared with the analogous electron decay measured for **1** on TiO₂ at 730 nm. The initial recombination kinetics measured on a picosecond timescale were also similar for the two dyes (Figure 6 inset).

The absence of a bleach also required quenching by iodide species to be monitored at a different wavelength for **2** / TiO₂. At 437 nm, in the presence of 0.25 or 0.5 M NaI, a long lived absorbance appears, which does **not** return to baseline before the next laser pulse arrives 50 ms later. The intensity of this absorbance increases as the monitoring wavelength is shifted toward 400 nm. These features are attributed to the formation of oxidized iodide species.¹⁴ The appearance of the absorbance is complete within the 14 ns instrument response. This implies a lower limit for the rate of I⁻ oxidation by **2**⁺ of 7×10^7 s⁻¹ at 0.5 M NaI concentration (1.4×10^8 M⁻¹ s⁻¹). We note that an I⁻ oxidation rate by Ru^{III}(dcb)(bpy)₂ anchored to SnO₂ of 1.2×10^{10} M⁻¹ s⁻¹ has recently been reported.¹⁴ An identical instrument response limited absorbance in the 400-440 nm range is observed for **2** anchored to SnO₂ in electrolyte. No transient is detected upon 532 nm photolysis of the electrolyte only, with no electrode present. Table 1 summarizes the rates of electron injection, recombination, and halide oxidation for the systems under study.

Table 1. Electron transfer rates at the sensitizer-semiconductor interface.

System	k_1^a s^{-1}	k_2^b $\times 10^{12} s^{-1}$	power mJ	k_{3a} 1 st order ^c $\times 10^7 s^{-1}$	k_{3b} 2 nd order $\times 10^8 s^{-1}$	α_a/α_b	k_4^d $\times 10^7 s^{-1}$
1 /TiO ₂	4.2 x 10 ⁷	> 2.9	0.05	0.4 ± 0.3	1.3 ± 0.4	0.15	>7.1
			0.11	1.2 ± 0.2	1.6 ± 0.1	0.48	
			0.25	1.3 ± 0.1	1.8 ± 0.1	0.62	
2 /TiO ₂	4.0 x 10 ⁹	> 2.9	0.20	0.4 ± 0.2	1.6 ± 0.4	0.36	>7.1
2 /SnO ₂	“	not meas'd	0.20	1.4 ± 0.1	3.2 ± 0.2	1.13	>7.1

a) Inverse excited state lifetime of the sensitizer dissolved in MeOH. b) Electron injection rate constant measured by time-resolved infrared absorbance. c) Injected electron-oxidized dye recombination analyzed according to the two component model described in the text. $k_{3b}(\text{observed}) = k_{3b}(\text{actual})/(\Delta\epsilon^*1)$. d) Dye reduction measured in a two-electrode cell with 0.5 M NaI and 0.05 M I₂.

Photoelectrochemistry. Steady-state photocurrents were measured for sensitized metal oxide electrodes in a two-electrode arrangement with 0.5 M NaI and 0.05 M I₂ electrolyte in propylene carbonate. Incident photon-to-current efficiencies (IPCE) are calculated using the following equation:

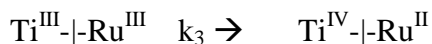
$$IPCE = \frac{(1240 \text{ eV} \cdot \text{nm})(\text{photocurrent density } \mu\text{A}/\text{cm}^2)}{(\lambda \text{ nm})(\text{irradiance } \mu\text{W}/\text{cm}^2)}$$

Dividing the IPCE by the fraction of incident photons absorbed at each wavelength (termed LHE, see Discussion section) gives the absorbed photon-to-current efficiency (APCE), shown in Figure 7 for **1** or **2** on TiO₂ or SnO₂. The uncertainty indicated is a convolution of the absorbance, photocurrent, wavelength and detector responsivity uncertainty. The latter dominates at high energy. The APCE for **2** improved significantly when the sensitizer was bound to SnO₂, and achieved a value of ≈ 40% independent of wavelength from 350 to 760 nm. Photocurrent measurements were performed primarily with illumination through the substrate side of the sensitized metal oxide electrodes. However, APCE spectra measured with “backside illumination” through the Pt counter electrode revealed no significant difference for wavelengths greater than 500 nm.

Discussion

As shown in the energy level diagram (Scheme 1) the ground state Ru^{III/II} oxidation potentials for **1** and **2** measured in solution are identical within experimental error.² Attempts to estimate the Ru^{III/II} potential for the compounds anchored to TiO₂ substrates by cyclic voltammetry have been unsuccessful. However, any shift upon surface attachment should be similar for these two closely related sensitizers. If the reduction potential of surface anchored **1**⁺ and **2**⁺ are in fact similar, one would expect similar rates of recombination (k_3) and halide oxidation (k_4). We have used a model which incorporates both a first order and second order recombination process to describe the observed recombination kinetics. The justification of this model is as follows:

Visible and EPR spectroscopy of electrochemically reduced TiO₂ films suggest a significant number of injected electrons reside in Ti^{IV} sites as Ti^{III}.¹⁵ For photo-injected electrons, the Ti^{III} species may be directly bound to the sensitizer. In this case the charge separated state and recombination reaction is depicted as



No diffusion of the reactants is required and the charge recombination should follow first order kinetics. A second possibility is that the electron diffuses away to a remote Ti^{IV} site before recombination occurs. This idea is consistent with the electron hopping mechanisms proposed for the conduction mechanism in colloidal anatase TiO₂ films.¹⁶ Under these conditions the recombination would resemble a bimolecular process where the electron must diffuse toward the oxidized sensitizer.



For this process, second order kinetics would be expected. Alternatively, self-exchange electron transfer across the nanocrystalline surface may shuttle the oxidized sensitizer away from the injection site, again leading to diffusion controlled recombination. An intellectually satisfying aspect of the proposed model is that the recovered 2nd order rate constant is generally independent of the excitation irradiance. For example, values of k_{3b} for **1**/TiO₂ in Table 1 are identical within experimental error for irradiances of 50 to 250 μJ. This is typically not true for the commonly used stretched exponential models.

The kinetics shown in Figure 6 and the recovered rates listed in Table 1 indicate similar recombination kinetics (k_3) for **1** and **2** anchored to TiO₂. It is concluded that **2**⁺ can effectively oxidize the iodide donors, primarily I⁻ and I₃⁻, within the several microsecond window of recombination. Quenching of the oxidized dye for **1**/TiO₂ in the presence of I⁻ and I₂, as shown in Figure 4, suggests the primary mechanism of dye reduction in working solar cells involves static quenching by I₃⁻.

We now turn to the competition between electron injection (k_2) and excited state decay (k_{-1}). The TRIR results in Figure 1 indicate that it is possible to lower the excited state potential³ by 200mV and still have < 350 fs electron injection. Two possible explanations for this behavior are: 1) the acceptors in the TiO₂ form a broad continuous energy band, overlapping well with both sensitizer excited state reduction potentials. 2) ultrafast electron transfer at these interfaces differs completely from the Marcus-Gerischer “weak electronic interaction” electron transfer and does not involve redistribution of vibrational excitation energy. In this case electron injection precedes excited state vibrational relaxation. The latter concept has been suggested by Willig and co-workers, who observed < 25 fs electron transfer from **1** to TiO₂ using an 1100 nm probe.^{1a} The smaller electron absorbance signal observed in the case of **2** suggests a ≈ 50% lower electron injection yield. From a kinetic standpoint, this is surprising. Even if the injection rate is as slow as 2.9 x 10¹² s⁻¹ (1/350 fs), it is still 3 orders of magnitude faster than the excited state decay of **2**, 4.0 x 10⁹ s⁻¹ measured in MeOH (Table 1). We therefore postulate that electron injection competes kinetically with vibrational relaxation to the thermally equilibrated state, rather than with radiative or non-radiative decay of the excited state.

A reduced injection yield for **2**/TiO₂ is also indicated by the transient visible spectroscopy. Spectra for **1** in Figure 2 indicate significant absorbance changes when the sensitizer is bound to TiO₂ vs. ZrO₂, attributed to **1** in the oxidized state and injected

electrons in TiO₂. For **2** the spectra on TiO₂ and ZrO₂, as well as in solution are remarkably similar, Figure 5. This suggests the majority of dye molecules are in the excited state, rather than in the oxidized form. However, when **2** is anchored to SnO₂, the excited state ligand absorbance at 400 nm disappears, an MLCT bleach is present, and near IR absorbance by injected electrons is evident. Thus, it is possible to achieve efficient injection from **2** by using an alternative semiconductor with lower energy acceptor states. It is unclear at this point whether the acceptors are the SnO₂ conduction band, Sn^{IV}, surface states, or a combination.

If recombination (k₃) is not a significant loss mechanism in the working solar cell, and the dye absorbance characteristics are known, then the yield of electron injection can be estimated through careful photocurrent measurements. The incident photon-to-current efficiency (IPCE) is a product of three terms:

$$IPCE = LHE * \phi_{inj} * \eta$$

Here LHE is the light harvesting efficiency or absorbance, defined as $LHE = 1 - 10^{-A}$ where A is the sample absorbance; ϕ_{inj} is the quantum yield for electron injection; and η is the efficiency of transporting injected electrons to the external circuit. It is well known that LHE is wavelength dependent, being related to the sensitizer absorbance spectra. The wavelength dependence of ϕ_{inj} and η are less certain. Dividing the IPCE by the LHE gives the absorbed photon-to-current efficiency (APCE), shown in Figure 7 for **1** and **2** anchored to TiO₂ or SnO₂.

$$APCE = \frac{IPCE}{LHE} = \phi_{inj} * \eta$$

Thus the APCE should reflect the wavelength dependence of ϕ_{inj} and η . For **1** on TiO₂ the APCE clearly drops off in the 600-700 nm range. When the same sensitizer is anchored to SnO₂, the APCE in the 400–600 nm range improves to 40% (vs. 20% on TiO₂) and actually *increases* from 600-700 nm. For **2** / TiO₂ the decrease in APCE at low energy is even more dramatic, and begins at 500 nm. For **2** / SnO₂ the APCE response is flat within experimental error, indicating efficient injection at all energies. With the exception of **2** / SnO₂, the shape of the APCE spectra indicate a wavelength dependence for ϕ_{inj} or η or possibly both. Transport efficiency (η) could be wavelength dependent if electrons injected at a greater distance from the conductive substrate (i.e. low energy photons with illumination through the ITO substrate) experienced greater loss during migration through the film. However, when the cell is illuminated from the back side^{16a,b} (through the Pt counter electrode) the APCE spectra are unchanged at $\lambda > 500$ nm. Thus, we conclude that the APCE spectra reflect the wavelength dependence of ϕ_{inj} . The results are consistent with a kinetic competition between electron injection and vibrational relaxation to the thermally equilibrated excited (thexi) state.¹⁷ A simple explanation for the wavelength dependence of ϕ_{inj} is that the vibrationally hot excited states of **1** and **2** can inject into TiO₂ while the thexi state cannot. The thexi state of **2** can apparently inject efficiently into SnO₂. The points of the initial decrease in APCE for **1** / TiO₂ and **2** / TiO₂ are 550 nm (2.3 eV) and 480 nm (2.6 eV). Note that the 0.3 eV energy difference is qualitatively similar to the 0.2 eV difference in excited state reduction potentials. The reason for the reproducible *increase* in injection efficiency for **1**/SnO₂ between 600 – 700

nm is not obvious. Perhaps a low energy surface state exists in SnO₂ which has enhanced orbital overlap with the excited state of **1** at this energy.

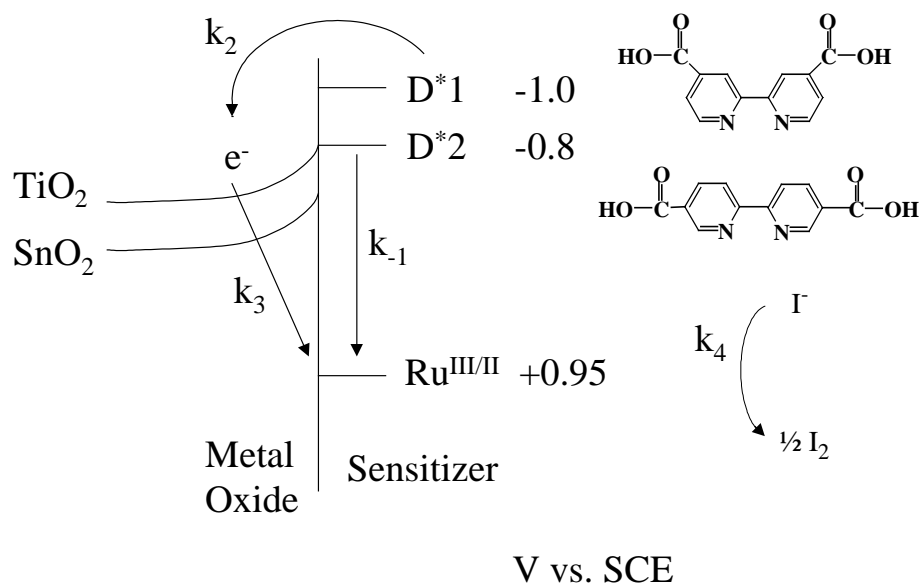
Moser and Graetzel have shown¹⁷ that for **1** / TiO₂, ϕ_{inj} is wavelength independent in the range 450 to 680 nm, but does decrease at $\lambda > 550$ nm for **1** / Nb₂O₅ where the conduction band lies 0.2 – 0.3 eV higher in energy. It is possible that our film preparation and other experimental conditions differ in such a way as to yield TiO₂ materials with acceptor states which are higher in energy than those studied by Moser. This could explain our observation of wavelength dependence for **1** / TiO₂.

The efficient sensitization of SnO₂ with **2** at all wavelengths of the MLCT absorbance band is encouraging, as sensitizer **2** holds particular promise for efficient solar cells. When the MLCT absorbance band is integrated over the AM 1.5 solar spectrum, an overall solar light harvesting efficiency of 27% is achieved. If a reasonable 80% of absorbed photons can be converted to electrons, as in the case of **1** and other sensitizers¹⁸ anchored to opaque TiO₂, an impressive 22% solar efficiency would result. We are currently attempting to prepare opaque, high surface area SnO₂ films in hopes of approaching this value.

Conclusions

A detailed set of time-resolved infrared, UV-VIS and photocurrent measurements for (4,4'dcb)₂Ru(NCS)₂ and (5,5'dcb)₂Ru(NCS)₂ adsorbed on ZrO₂, TiO₂ and SnO₂ nanocrystalline film substrates have been performed. These studies were conducted with the aim of identifying inherent electron transfer processes responsible for an observed difference in photon-to-electron efficiencies for the above sensitizers in photoconductive TiO₂ solar cells. Ultrafast injection rates for both dyes on TiO₂ suggest that wavelength-dependent cell efficiencies are probably governed by coupling of the donor excited state levels with appropriate accepting levels of the substrate, back electron transfer and redox couple quenching rates. To this end, measurements were conducted to monitor transient UV-VIS spectra and kinetics to identify the competition between back electron transfer and oxidized dye quenching by added iodine electron donors (e.g., I, I₃⁻) as a function of iodine ion concentration.

We also showed that absorbance-corrected photocurrent measurements provide useful determinations of electron injection and transport yields. The results indicate that when donor/acceptor overlap is less than ideal, sensitizer excited state vibrational relaxation can compete with ultrafast electron injection. Most importantly, it has been demonstrated that efficient electron injection over the 350-800 nm wavelength range can be achieved with the red-shifted sensitizer (5,5'dcb)₂Ru(NCS)₂. This was accomplished by employing SnO₂ as an alternative semiconductor to TiO₂ since it apparently has energy acceptor states that overlap well with sensitizer lower-energy donating levels. Even under these conditions, the injected substrate electron-to-sensitizer recombination rate is not significantly affected and, based on our observations, solar cells constructed with either dye on transparent SnO₂ substrates are expected to function with extremely high photon-to-electron conversion efficiencies.



Scheme 1

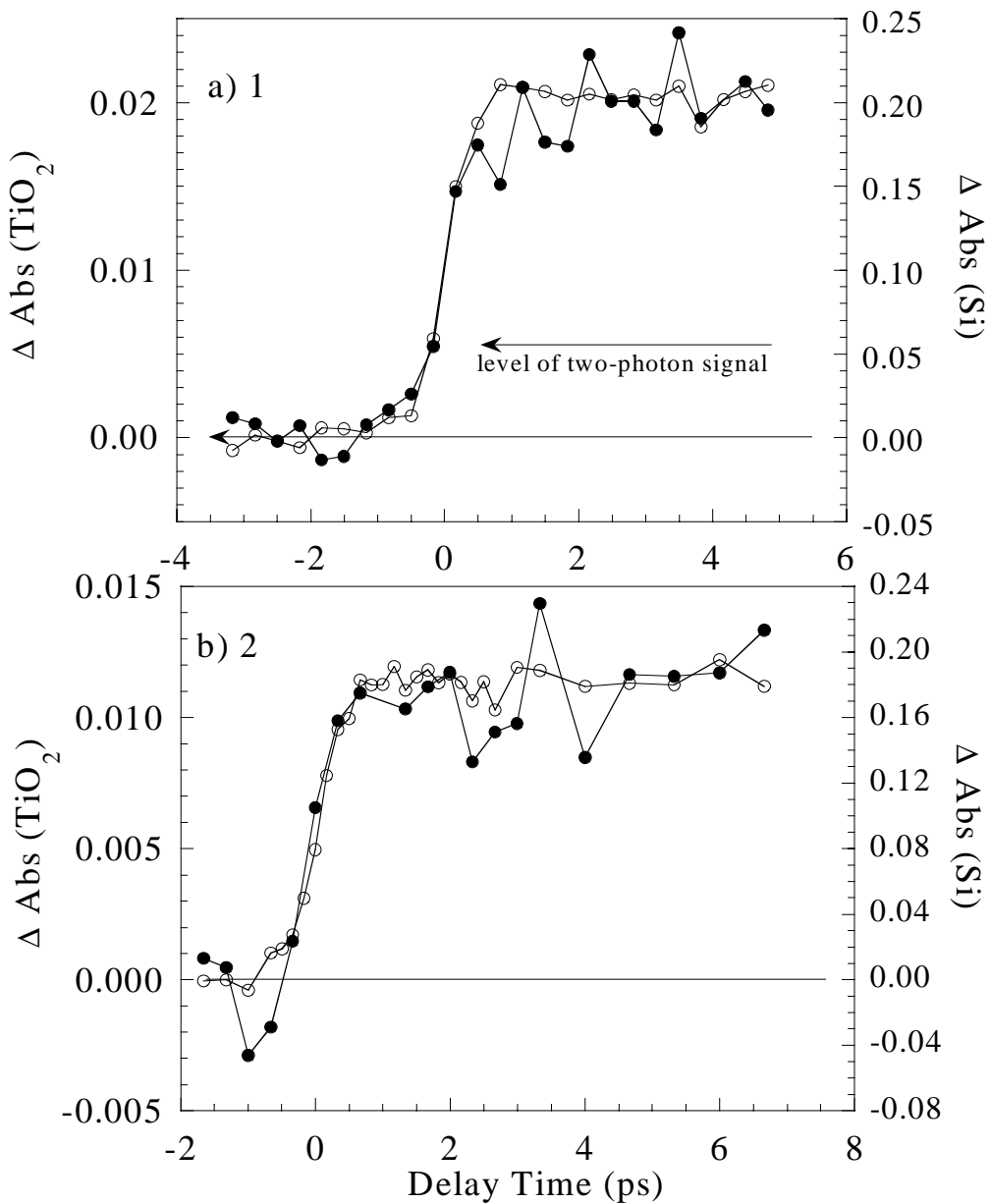


Figure 1. Rise-time of the TiO₂ electron absorbance at 5.4 μm for a) **1** and b) **2** sensitized TiO₂ films in dichloromethane. Open circles indicate pump-probe cross-correlation measured in a Si wafer. Closed circles indicate absorbance by the injected electrons for sensitizers on TiO₂.

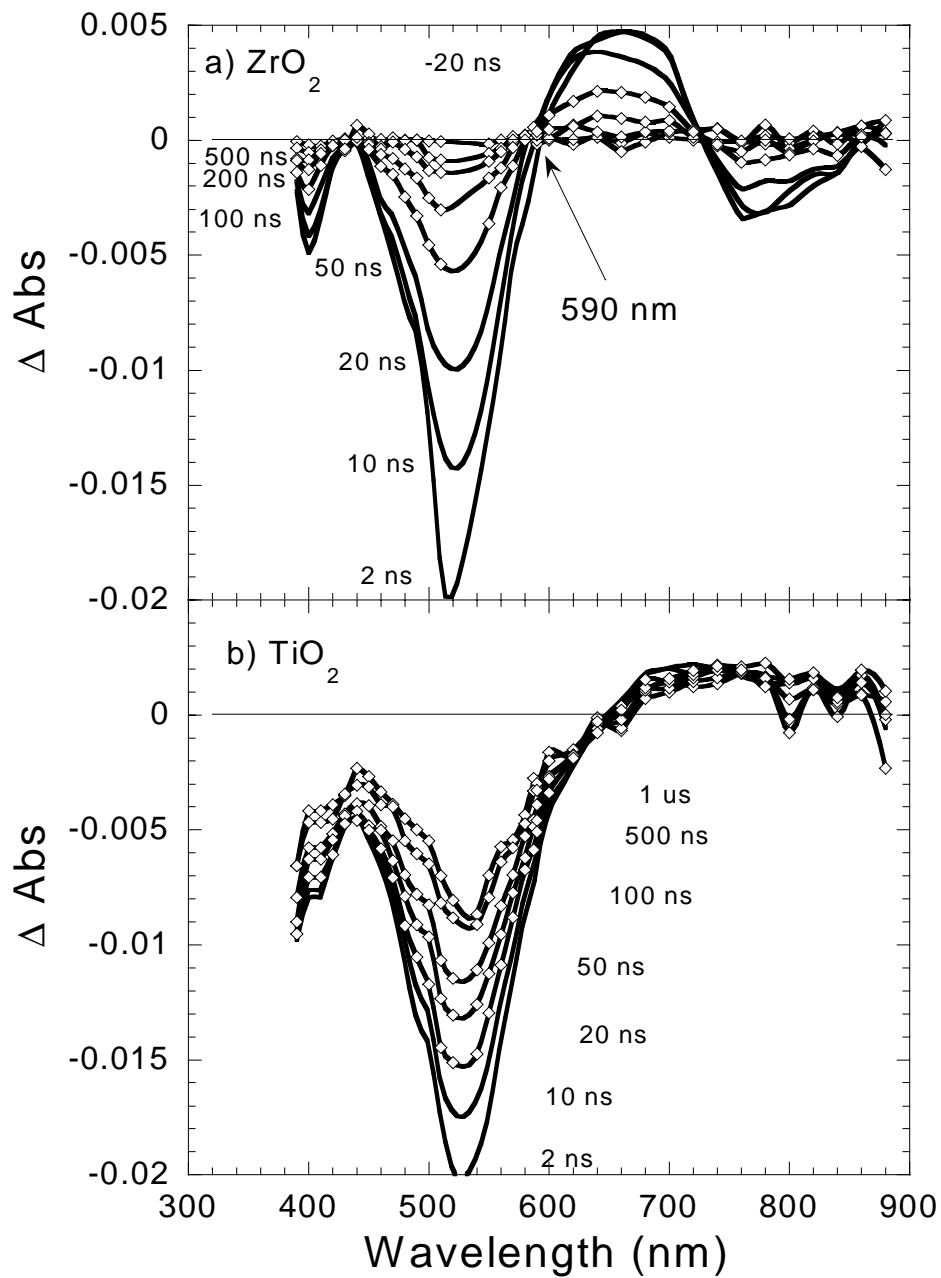


Figure 2. Transient visible absorbance difference spectra, uncorrected for photoluminescence of a) ZrO_2 and b) TiO_2 films sensitized with **1** under 532 nm, 0.1 mJ excitation.

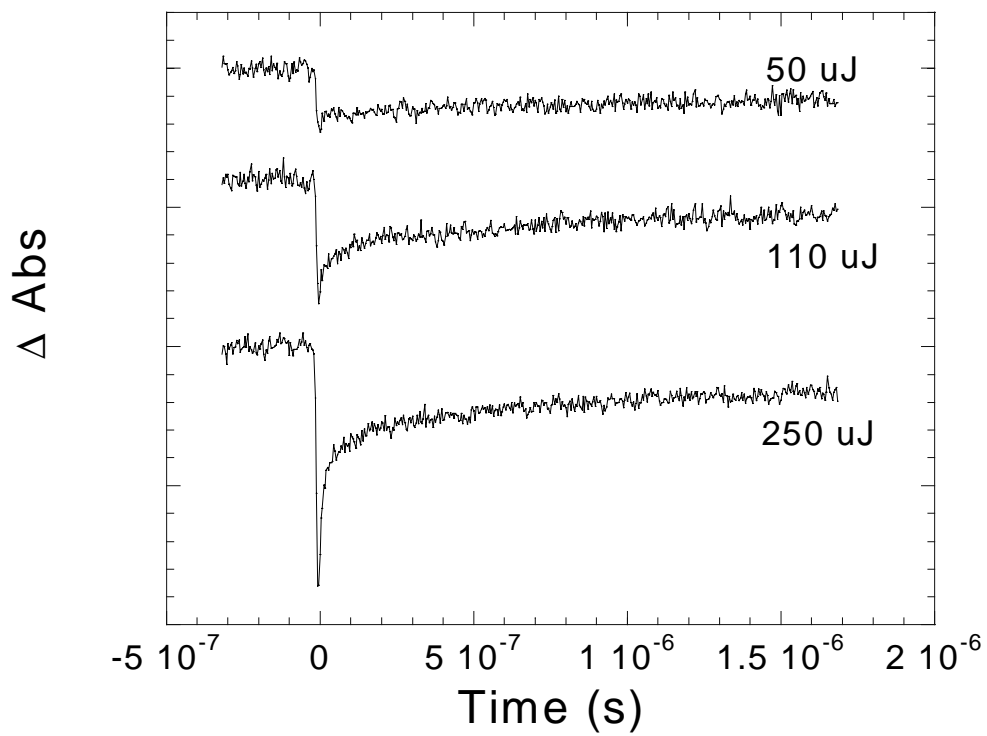


Figure 3. Oxidized dye – injected electron recombination kinetics measured at 590 nm for **1** anchored to TiO_2 , as a function of excitation irradiance at 532 nm.

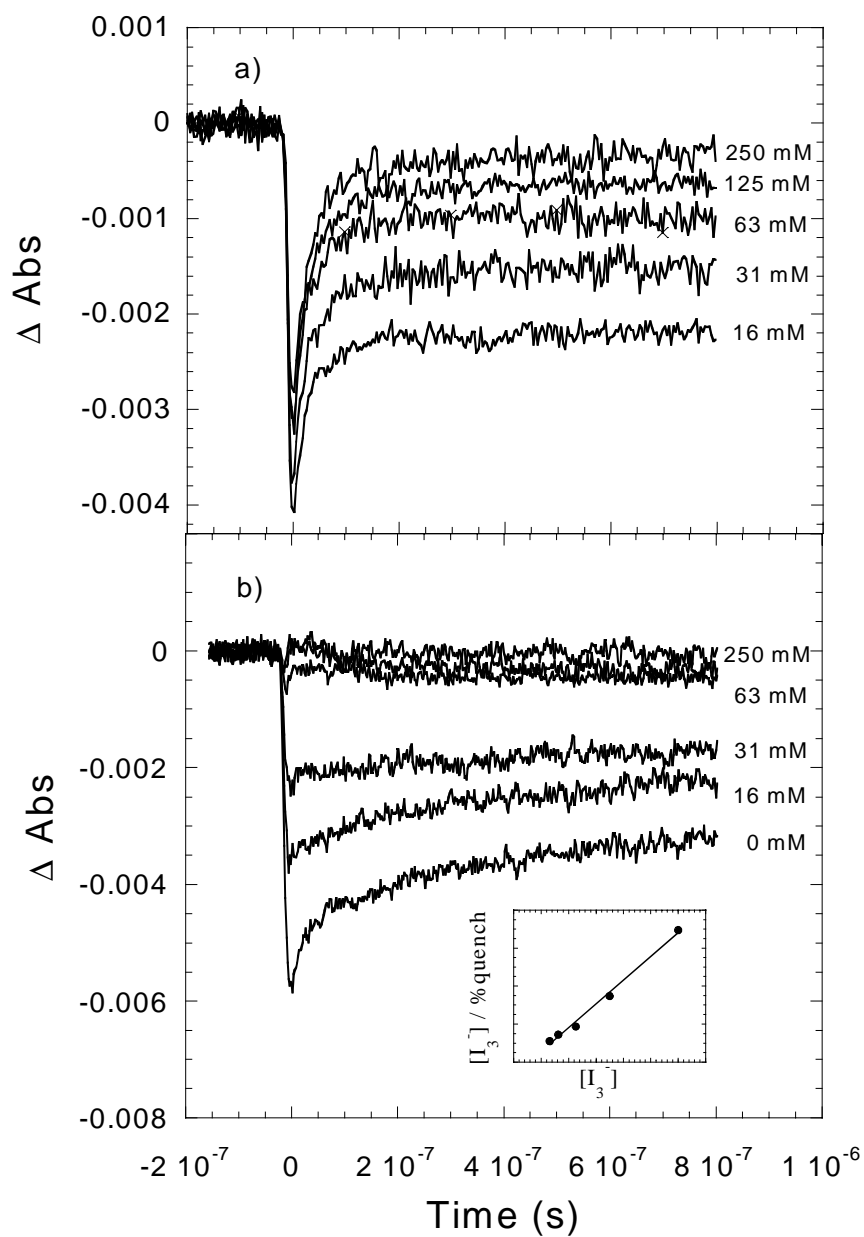


Figure 4. Quenching of oxidized **1** as a function of added **a)** NaI or **b)** NaI and I₂ in a 10:1 molar ratio, measured at 590 nm under 0.2 mJ, 532nm excitation. The molarity of NaI is indicated. The inset shows a fit to the Langmuir adsorption isotherm model in terms of $[\text{I}_3^-]$ as described in the text.

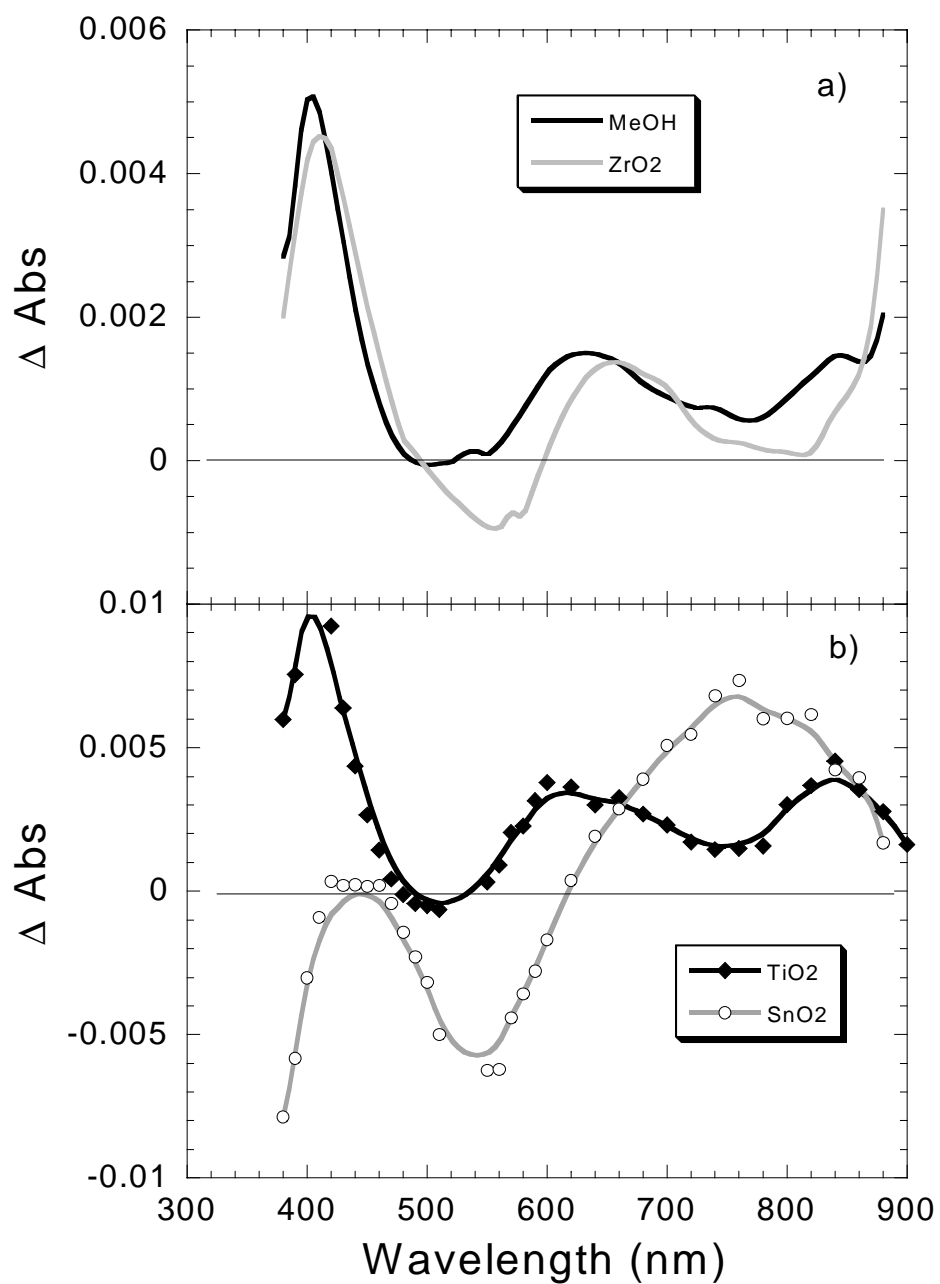


Figure 5. Transient visible absorbance spectra of **2** in MeOH or on ZrO₂ (a) and on TiO₂ or SnO₂ films (b). Spectra shown were taken at 5 ns following 532 nm, 0.1 mJ excitation for films or 570 nm excitation in MeOH.

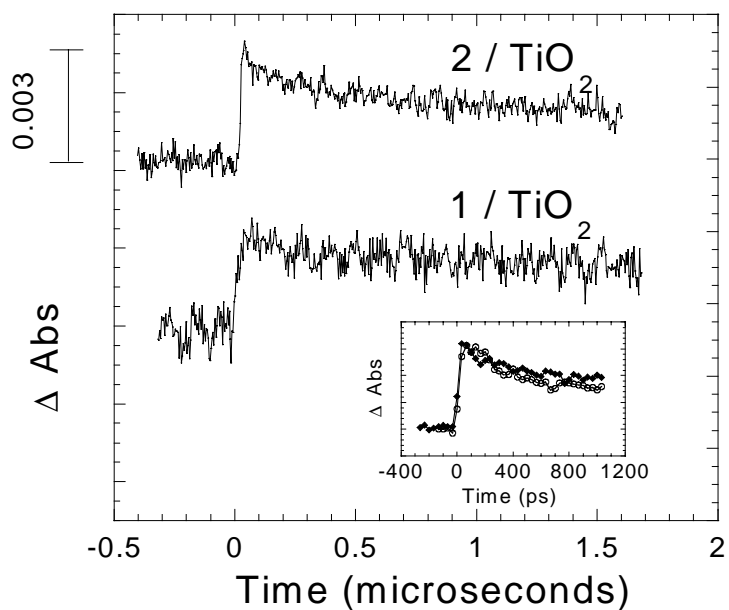


Figure 6. Oxidized dye – injected electron recombination kinetics measured at 730 nm for **1** and 820 nm for **2** anchored to TiO₂. Probe wavelengths were chosen to eliminate or minimize contributions from the sensitizer excited state. Excitation irradiance was 0.1 mJ for **1** and 0.2 mJ for **2** such that an approximately equal number of electrons were injected in each case. Kinetics measured on a picosecond timescale are shown in the inset for **1** (closed symbols) and **2** (open symbols).

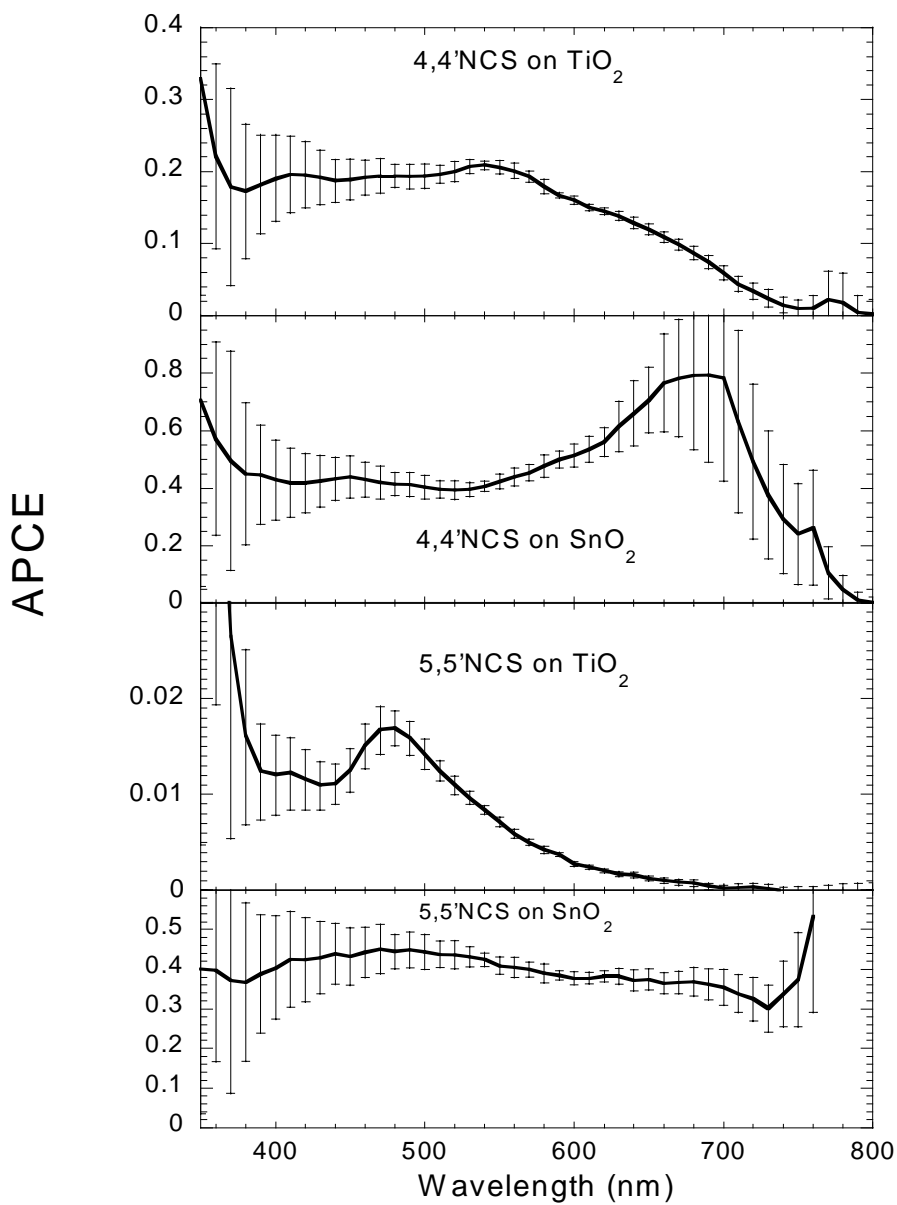


Figure 7. Photon-to-current conversion efficiency for sensitized metal oxide electrodes in a two-electrode solar cell with NaI/I₂ electrolyte. Efficiencies are corrected for the fraction of incident photons absorbed by the sensitizer at each wavelength, see text for details.

References

- ¹ a) Hannappel, T.; Burfeindt, B.; Storck, W.; Willig, F. *J. Phys. Chem. B*, **1997**, *101*, 6799. b) Heimer, T.A.; Heilweil, E.J. *J. Phys. Chem. B* **1997**, *101*, 10990. c) Ellingson, R.J.; Asbury, J.B.; Ferrere, S. Ghosh, H.N.; Sprague, J.R.; Lian, T.; Nozik, A. *J. Phys. Chem. B* **1998**, *102*, 6455.
- ² Argazzi, R.; Bignozzi, C. A.; Heimer, T. A.; Castellano, F. N.; Meyer, G. J. *Inorg. Chem.* **1994**, *33*, 5741.
- ³ Ground state Ru^{III/II} potentials were reported in reference 2. In the absence of emission from the fully protonated form of **2**, we have estimated the E₀₀ energy for both sensitizers from the low energy absorbance onset. The excited state reduction potential D* is calculated as D* = E_{1/2}(Ru^{III/II}) - E₀₀. This analysis yields D* = -1.0 and -0.8 V vs. SCE for **1** and **2** respectively.
- ⁴ a) Gerischer, H. *Pure and Appl. Chem.* **1980**, *52*, 2649. b) Fessenden, R.W.; Kamat, P.V.; *J. Phys. Chem.* **1995**, *99*, 12902.
- ⁵ O'Regan, B.; Moser, J.; Anderson, M.; Graetzel, M. *J. Phys. Chem.* **1990**, *94*, 8720.
- ⁶ Heimer, T. A.; D'Arcangelis, S. T.; Farzad, F.; Stipkala, J. M.; Meyer, G. J. *Inorg. Chem.* **1996**, *35*, 5319.
- ⁷ Lemon, B.I.; Hupp, J.T. *J. Phys. Chem. B* **1997**, *101*, 2426.
- ⁸ Disclaimer: Certain commercial equipment, instruments, or materials are identified in this paper in order to adequately specify the experimental procedure. In no case does such identification imply recommendation or endorsement by the National Institute of Standards and Technology, nor does it imply that the materials or equipment identified are necessarily the best available for the purpose.
- ⁹ Heimer, T.A.; Heilweil, E.J. *Ultrafast XI*, Springer-Verlag, **1998**, pg 505.
- ¹⁰ a) Heilweil, E. J.; Cavanagh, R. R.; Stephenson, J. C.; *Chem. Phys. Lett.* **1987**, *134*, 181. b) Dougherty, T. P.; Heilweil, E. J. *Optics Letters* **1994**, *19*, 129.
- ¹¹ The Si photodiode was calibrated following the procedure in NIST special publication 250-41: *Spectroradiometric Detector Measurements*, Larason, T.C.; Bruce, S.S.; Parr, A.C.
- ¹² Published spectra vary at wavelengths greater than 700 nm, due to differences in photoluminescence collection efficiency. See for example Tachibana, Y.; Moser, J.E.; Graetzel, M.; Klug, D.R.; Durrant, J.R. *J. Phys. Chem.* **1996**, *100*, 20056.
- ¹³ Haque, S.A.; Tachibana, Y. Klug, D.R.; Durrant, J.R.; *J. Phys. Chem. B* **1998**, *102*, 1745.
- ¹⁴ Nasi, C.; Hotchandani, S.; Kamat, P.V. *J. Phys. Chem. B* **1998**, *102*, 4944.
- ¹⁵ a) Cao, F.; Oskam, G.; Searson, P.C.; Stipkala, J.M.; Heimer, T.A.; Farzad, F.; Meyer, G.J. *J. Phys. Chem.* **1995**, *99*, 11974. b) Rothenberger, G.; Fitzmaurice, D.; Graetzel, M. *J. Phys. Chem.* **1992**, *96*, 5983.
- ¹⁶ a) Soedergren, S.; Hagfeldt, A.; Olsson, J.; Lidquist, S.-E. *J. Phys. Chem.*, **1994**, *98*, 5552. b) Rensmo, H.; Linstrom, H.; Soedergren, S.; Lindquist, S.-E. in *Nanostructured Materials in Electrochemistry*; Searson, P. C., Meyer, G. J., Eds.; The Electrochemical Society: New Jersey, 1995, Vol. 95-8, p. 67. c) Oskam, G.; Cao, F.; Searson, P.C. *ibid*; p. 98.
- ¹⁷ Moser, J.E.; Groetzel, M. *Chimia*, **1998**, *52*, 160.
- ¹⁸ a) Nazeeruddin, M.K.; Kay, A.; Rodicio, I.; Humphry-Baker, R.; Mueller, E.; Liska, P.; Vlachopoulos, N.; Graetzel, M. *J. Am. Chem. Soc.* **1993**, *115*, 6382. b) Nazeeruddin, M.K.; Liska, P.; Moser, J.; Vlachopoulos, N.; Graetzel, M. *Helv. Chim. Acta* **1990**, *73*, 1788.